nature | methods

Plasma membrane topography and interpretation of single-particle tracks

J Adler, A I Shevchuk, P Novak, Y E Korchev & Ingela Parmryd

Supplementary figures and text:

Supplementary Figure 1	HPICM, speed of image acquisition varies with number of pixels.
Supplementary Figure 2	SICM images of small areas of live cells.
Supplementary Figure 3	SICM images of live cells.
Supplementary Figure 4	Pillars reduce the apparent movement of single particles.
Supplementary Figure 5	Simulating diffusion on a non-flat surface.
Supplementary Figure 6	Apparent topography trapping is indistinguishable from binding sites.
Supplementary Table 1	Cell types imaged by ion conductance microscopy.
Supplementary Note	Supplementary discussion and protocols

Supplementary Figure 1. HPICM, speed of image acquisition varies with number of pixels.

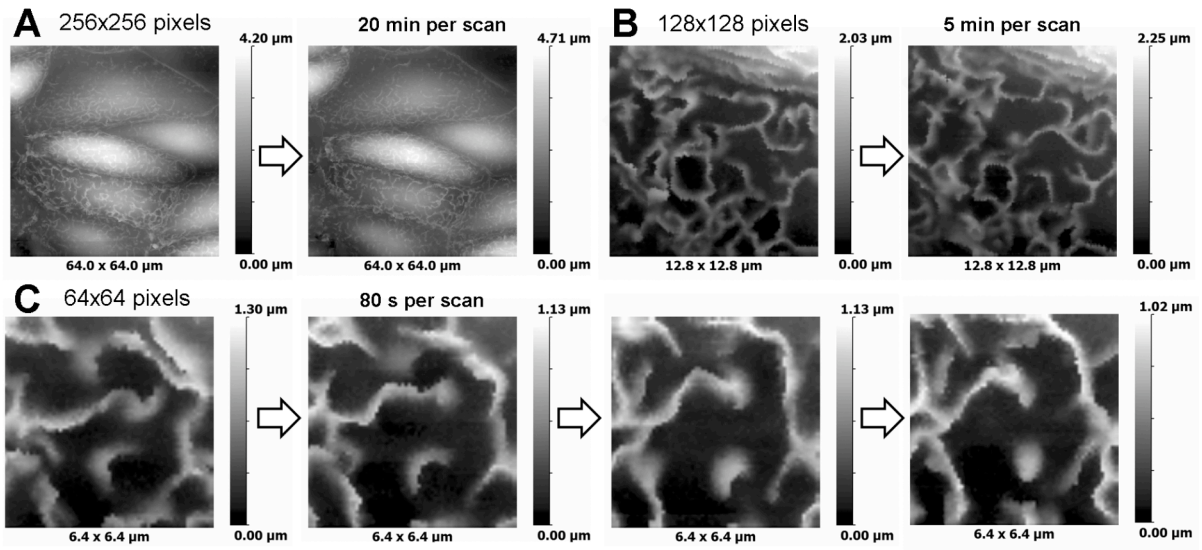

Dynamics of ridges in living epithelial cells. (**a**) Topographical HPICM images of a cell monolayer. Each 256x256 pixel image was acquired in 20 min. (**b, c**) Dynamics of ridges in living epithelial cells. Each 128x128 pixel image in B was acquired in 5 min. Each 64x64 pixel image in C was acquired in 80 sec.

Supplementary Figure 2. SICM images of small areas of live cells.

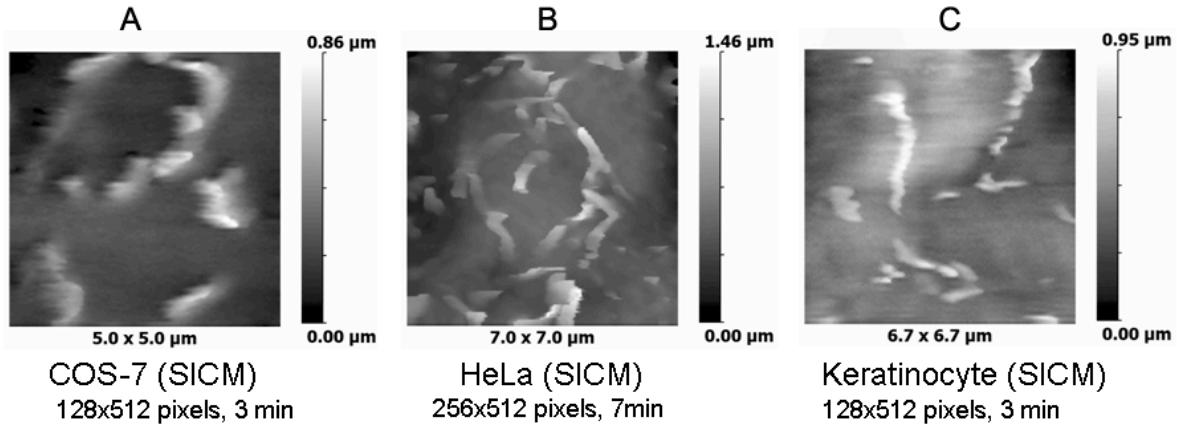

(**a**) A live COS-7 cell (128x512 pixels, 3 min per scan). Cells were prepared as described (Shevchuk, A. I., P. Hobson, M. J. Lab, D. Klenerman, N. Krauzewicz, & Y. E. Korchev. 2. *Pflugers Arch.* **456**, 227-235 (2008)). (**b**) A live HeLa cell (256x512 pixels, 7 min per scan) and (**c**) a live keratinocyte (128x512 pixels, 3 min per scan).

Supplementary Figure 3. SICM images of live cells.

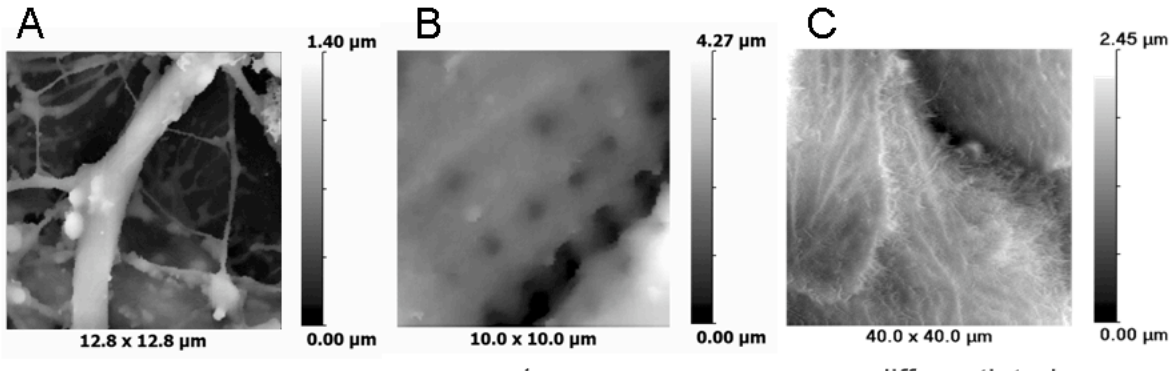

(**a**) HPICM image (256x256 pixels) of hippocampal neurons. Scan took 16 min. Cells were prepared as described (Shah, M. & Haylett, D. G. J. Neurophysiol. 83, 2554-2561, 2000). (**b**) HPICM image (128x128 pixels) of a rat ventricular cardiomyocyte. Scan took 9 min. Cells were prepared as described (Harding, S. E., Vescovo, G., Kirby, M., Jones, S. M., Gurden, J. & Poole-Wilson, P. A. *J. Mol. Cell. Cardiol.* **20**, 635–647 (1988)). (**c**) ICM image (256x512 pixels) of an undifferentiated human embryonic stem cell NCL1 line (hES-NCL1) growing on precoated cover slip with human serum as described previously (Stojkovic, P et al. *Stem Cells* **23**, 895-902 (2005)). Scan took 17 min. hES-NCL1 cells were imaged by Dr Julia Gorelik.

Supplementary Figure 4. Pillars reduce the apparent movement of single particles.

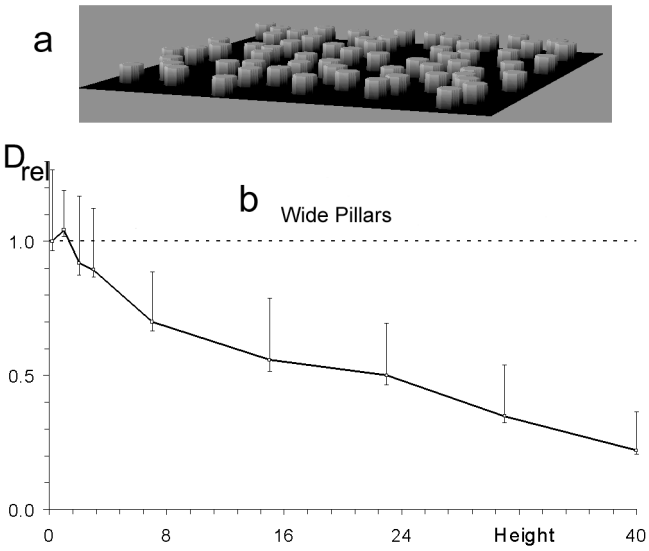

(**a**) Pillars with a radius of eight pixels with different height were randomly inserted onto a 256,256 pixel flat surface, covering 14% of the horizontal surface. (**b**) Single particles were inserted randomly onto the surface and their movement followed. The diffusion coefficient relative to that for a flat surface is shown along with error bars for both the SD (above) and SEM (below) as the height of the pillars is altered, $N \geq 32$. The same array of pillars was used in all simulations.

Supplementary Figure 5. Simulating diffusion on a non-flat surface.

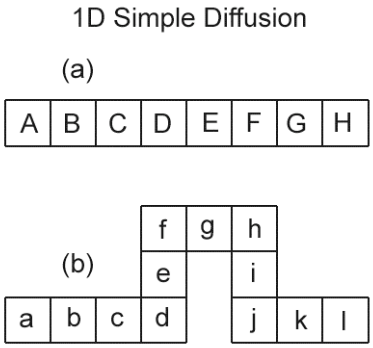

The simulation of diffusion over a non-flat surface used a sheet of connected pixels where the connections could be within the plane or to adjacent pixels above or below the plane. This is illustrated by comparing a straight 1D connected series of pixels (**a**) with a series of connected pixels that include a kink (**b**). In each case the pixels, except the two at the ends, have two neighbours to which a move can be made. The 2D the arrangement is similar, although each pixel has four rather than two neighbours. In terms of modelling diffusion the particle randomly selects from the four available neighbouring pixels.

Supplementary Figure 6. Apparent topography trapping is indistinguishable from binding sites.

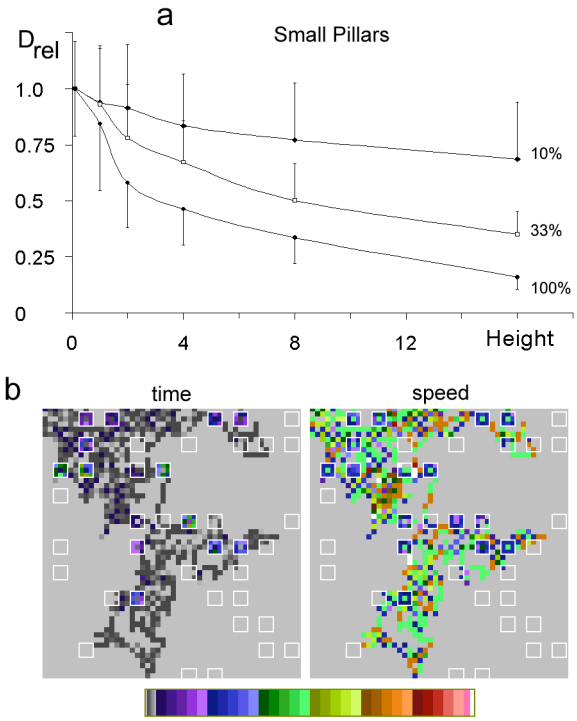

(**a**) The surface was subdivided into an array of 5x5 pixel sites and these sites were filled with a hollow 3x3 pixel column with a flat top. The height and number of pillars was varied and expressed as the fraction of the possible sites that were filled; 10%, 33% or 100%. The same three arrays were used in all the simulations. The XY coordinates were used to calculate diffusion coefficients, relative to diffusion over a flat surface. Error bars display the SD and are shown in one direction for clarity, N=32. (**b**) The residence time and speed are shown for a single particle on pillars 16 voxels high. The false colour scale covers a range of speeds from 0 to 4 pixels/cycle and total residence times from 0 to 90 cycles, each cycle consisting of four random moves.

Supplementary Table 1. Cell types imaged by ion conductance microscopy.

Cell group	Cell type
Endothelial cell	Human umbilical vein primary culture
Epithelial cells	Xenopus kidney epithelial A6 Caco-2- human colonic carcinoma MDCK (Madin-Darby canine kidney) AT1 human alveolar type
Muscle cells	Human ventricle cardiac myocytes Rat ventricle cardiac myocytes Rabbit ventricle cardiac myocytes Guinea pig ventricle cardiac myocytes Mouse ventricle cardiac myocytes Neonatal Rat cardiac myocytes Guinea pig gut smooth muscle Rat skeletal muscle
Neuronal cells	Rat Hippocampal Neurons Neuroblastoma cells DRG Astrocytes
Sperm cells	Boar Human Mouse Sea urchin
Blood cells	Lymphocytes Neutrophils Erythrocytes
Bone cells	Neonatal rat long bone osteoblasts Neonatal rat long bone osteoclasts Human bone marrow
Hair cells	Mouse corti inner hair Mouse corti outer hair Mouse corti Hensen's Mouse corti outer phalangeal Mouse corti inner pillar Mouse corti outer pillar Mouse corti Claudius
Stem cells	hESC-NCL1(human Embryonic Stem Cell -derived neuronal) hESC-derived cardiomyocytes hESCs (H7 line) Human neural crest-like SCs derived Melanoblast

	Pre-Schwann Condrocytes Sensory neuron subtypes Melanocyte
Oocyte	Xenopus
Breast cancer cell lines	MCF-7 (human) ZR751 (human) MDA-231 (human adenocarcinoma)
Miscellaneous cell lines	COS-7 - African Green Monkey SV40-transfected kidney fibroblast CV-1- derived from Cercopithecus aethiops monkey kidneys CHO- *Chinese hamster ovary* 3T3- Swiss mouse embryo fibroblasts HEK293- human embryonic kidney HeLa- cervical cancer cells from Henrietta Lacks PTK- adult male rat kangaroo kidney (Potorous tridactylus) PC12 - rat adrenal medulla pheochromocytoma FRSK – fetal rat skin keratinocytes NRK – normal rat kidney epithelial Pituitary
Tissue	Human umbilical vein Rat aorta Rat optic nerve Rat hippocampal slice Rat cerebellum slice
Bacteria	Escherichia coli Shewanella Streptococcus Streptomyces
Insect	Drosophila eye
Plant	Onion epidermis Potentilla rupestris flower leaf

Supplementary Discussion

Alignment of the Surface and the Imaging Plane

Accurate analysis of SPT requires that the surface is flat and that the surface is aligned with the imaging plane of the microscope. The former is discussed in the main article but alignment is a separate issue. If a flat surface is not aligned with the imaging plane and particles are only localized in 2D then distances measured between successive positions along the direction of the misalignment will be under reported. The practical question is whether a degree of misalignment that would affect SPT measurements can be detected by widefield microscopy. Misalignment would be expected to manifest itself as anisotropic movement, whether this would be interpreted as misalignment or as an interesting feature of the surface is less obvious. Topography is important.

Diffusion on Non-Flat Surfaces with Regular Geometry

There is a body of work on the effects of regular geometric perturbations on surfaces and the consequences for the measurement of movement[1-3] which, in our opinion, has not received appropriate acknowledgement. These show that topography is important and that corrections could be made for diffusion measurements if the topography was regular and known. We have examined the surface of cells using a high resolution imaging technique and examined how topography affects a simple single particle diffusion simulation. Cells do not have a regular geometry and the real goal is not to correct global measures of diffusion, which is of course worthwhile, but to correct local measures of movement and disentangle the interaction of particles with inhomogeneities in the plasma membrane.

Diffusion on Irregular and Locally Rough Surfaces

Wieser and Schutz[4] consider geometries that lead to an apparent subdiffusion behavior and consider how, in the context of hop diffusion, a variability in domain sizes is a further complication that can easily lead to misinterpretation; '*researchers would no doubt ascribe such results to anomalous subdiffusion*'. They also consider that a moving domain model can yield the same results as hop diffusion.

Locally rough surfaces have been examined by Hall[5], finding that 'surface roughness effects can distort the results gained from a conventional analysis of such membrane SPT measurements that does not account for such effects'. The conventional analysis is of course 2D. A scheme is also proposed for measuring roughness using single molecule tracking over an entire cell and using the autocorrelation of repeated local measurements to infer relative surface roughness.

King[6] uses a two dimensional crested cycloid to create simulated surfaces for random walks, which are then analysed in 2D. The measured diffusivity decreases as a function of membrane area.

Limitations of HPICM.

Like all scanning probe microscopes speed is a limitation (**Supplementary Fig. 1**) and it is possible that the plasma membrane could move during the time required to acquire a complete image. This is to some extent compensated for by the acquisition of images as a series of square blocks and their assembly into a complete image. This ensures that adjacent pixels are acquired almost concurrently and therefore have correct relative heights. In the context of SPT if the plasma membrane moves during the particle tracking the interpretation of tracks becomes appreciably harder. If multiple particles are being tracked concurrently any overall movement of the cell is likely to be detected by a common motion, but if small areas of the membrane are independently motile, say a short projection retracting, then this will be

very difficult to spot. An additional limitation of scanning probe microscopy is the inability to follow reentrant parts of the surface, like the right hand portion of surface shown in Fig. 1e. This may lead to an underestimate of the surface area.

Tags and Molecules

In the main article (**Fig. 1e**) it is pointed out that SPT frequently follows a tag, nanogold, quantum dot or a fluorescent protein, rather than the molecule of interest and that the location of the molecule must be offset from the centre of tag by the radius of the tag, which for a large nanogold particle may be 20 nm. On a horizontal surface it is possible that the tag and molecule of interest maintain a fixed alignment, in which case there will be a constant offset and movements of the tag reflect movements of the molecule. However once it is accepted that surfaces are not smooth (**Fig. 1e**), even if a tag maintains a fixed alignment relative to the surface, movements of the tag no longer precisely match movements of the molecule of interest and the distance measured between successive locations is in error by up to ± the diameter of the tag. These are potentially very significant errors and might be expected to have a relatively greater impact over short distances. This additional and unrecognized source of error resembles that reported by Martin et al.[7], who demonstrated that SPT on a flat surface showed subdiffusion in conditions when only simple diffusion was possible. The source of the anomaly was the cumulative effect of errors in locating the diffusing particles. Localisation errors are a recognised problem and estimates of the size of the errors are generally obtained by repeatedly imaging an immobilized tag or theoretically[8] and are incorporated into the analysis of SPT. However difference between the location of the tag and the molecule of interest is an additional problem.

The problem becomes appreciably worse if the assumption that the tag retains a fixed alignment with respect of the surface does not hold. This could be due to flexible link to the molecule of interest. A mismatch between a tag and the molecule of interest in electron microscopy studies was considered by Parton and Hancock[9] along with the additional spacing produced by a linking antibody.

The relationship between surface area and diffusion rate

Our basic premise is that the plasma membrane is not flat and therefore when the shortest path is calculated between successive positions of a single particle, that was only tracked in 2D, the distance will understate the actual path. The degree of understatement depending upon the topography of the surface. If the surface area was sufficient to halve the calculated distances the corresponding diffusion coefficient will fall by a factor of four, since the diffusion coefficient is based on the mean square deviation (MSD). The relevant questions are what is the surface area and topography of live cells. Studies on Xenopus oocytes indicate that cells can have as much as ten times more plasma membrane than that predicted from assuming a smooth sphere[10]. This implies that we are only scratching the surface of an iceberg when measuring a threefold decrease in diffusion rates (**Fig. 1b-c**) and that a lot more detail is likely to be revealed as the resolution of HPICM is improved.

FRAP and Diffusion on the Plasma Membrane

FRAP, unlike SPT, produces an average result for all mobile molecules and has been used to examine the movement on the plasma membrane[11]. The authors of this particular study assumed that the membrane was flat and did not consider that any of their experimental interventions might affect membrane topography. They simply concluded that the slower diffusion seen the plasma membrane is an intrinsic property of the membrane. In contrast is Wolf et al.[12] who examine the effect of microvilli on diffusion, for which they found little effect. An unexpected result but connected to the immobile fraction of the fluorophore which

is presumably on the microvilli and able to contribute little to the replenishment of the photobleached area. This is a systematic problem with FRAP which is too focused on relatively rapid changes and does not consider the timescale over which the 'immobile' fraction is replenished.

FCS and Topography

FCS examines the fluctuations in fluorescence in a small volume, the volume being determined by a stationary focused laser beam and from which photons are emitted. When FCS is used to examine the plasma membrane the issue is the amount and orientation of the membrane within the excitation volume, even with STED[13] the volume within which excitation is possible is large compared to the thickness of the plasma membrane (4-5 nm). If the membrane is flat and aligned with the imaging plane then a small volume of membrane is being studied which will remain constant as different areas are examined. But if the membrane is not flat the volume and its orientation within the excitation volume will vary substantially.

Overall, the importance of our caution is underscored by a recent and extensive review on membrane microdomains[14]. The “mechanisms that impede free diffusion in cell membranes”, as measured by SPT, FRAP and FCS, are discussed but topography, which adds another level of complexity, is ignored.

Supplementary Methods

Cell Culture

FRSK cells from the Japanese Collection of Research Bioresources were cultured in MEM medium supplemented with 10% heat-inactivated FCS, 2 mM L-glutamine, 100 U/ml penicillin and 100 g/ml streptomycin (complete medium) in a humidified incubator under 10% CO_2. Live cells were imaged in complete media with the FCS replaced with 25 mM HEPES.

Fixation was performed in 0.75% glutaraldehyde in filament preserving buffer (1% Triton X-100, 137 mM NaCl, 5 mM KCl, 1.1 mM Na_2HPO_4, 0.4 mM KH_2PO_4, 4 mM $NaHCO_3$, 5.5 mM glucose, 2 mM $MgCl_2$, 2 mM EGTA, 5 mM PIPES pH 6.0) for 15 minutes at 37ºC[15].

A single kidney epithelial A6 cell line was kindly provided by Dr. P. DeSmet (Karnolieke Universiteit, Belgium). All experiments were carried out between 127 and 134 passages. Cells were cultured as described previously[16]. They were kept in a growth medium consisting of one part modified Ham's F-12 and one part Leibovitz's L-15 modified to contain 105 mM NaCl and 25 mM $NaHCO_3$ (1:1) (Gibco, Parsley, UK). The mixture was supplemented with 10% fetal calf serum (Gibco), 200 mg/ml streptomycin and 200 U/ml penicillin (Gibco). Cells were maintained at 28ºC in an atmosphere of humidified air plus 1% CO_2.

HPICM Setup

All experiments were performed using a SICM scanner controller (Ionoscope, UK) and scan head (Ionscope, UK). Two different heads were used for imaging. Scan head #1 consisted of a PIHera P-621.2 XY Nanopositioning Stage (Physik Instrumente (PI), Germany) with 100 x 100 μm travel range that moved the sample and a LISA piezo actuator P-753.21C (PI) with travel range 25 μm for pipette positioning along the Z-axis. Coarse positioning was achieved with translation stages M-111.2DG (XY directions) and M-112.1DG (Z-axis) (PI). The Z piezo actuator was driven by a 200 W peak power low voltage PZT amplifier E-505 (PI), while the XY nanopositioning stage was driven by 3 x 14 W amplifier E-503 (PI). Scan head #2 consisted of a P-733.2DD Ultra-High-Speed, XY Scanning Microscopy Stage (PI) customized for 10 x 10 μm travel range (XY movement of the sample) and a LISA piezo actuator P-753.21C customized for 5 μm travel range (PI) that moved the nanopipette along Z-axis. A translation stage M-112.1DG with a travel range of 25 mm (PI) was used for coarse positioning of the pipette in the Z-axis. All piezos were driven by 200 W peak power low voltage PZT amplifiers E-505 (PI).

All piezo elements in both scan heads operated in capacitive sensor-controlled closed loop using Sensor & Position Servo-Control Module E-509 (PI). Scan heads were placed on the platform of inverted Nikon TE200 microscope (Nikon Corporation, Japan). The pipette current was detected via an Axopatch 200B (Molecular Devices (MD, USA) using a gain of 1 mV/pA and a low-pass filter setting of 5 kHz. The internal holding voltage source of the Axopatch-200B was used to supply a DC voltage of +200 mV to the pipette. The outputs of the capacitive sensors from all three piezo elements were monitored using Axon Digidata 1322A (MD) and Clampex 9.2 (MD).

HPICM probes

Nanopipettes were pulled from borosilicate glass (O.D. 1 mm, I.D. 0.58, Intracell, UK) using a laser-based puller Model P-2000 (Sutter Instruments Co., USA). Two different pipettes were used: Standard pipettes, displayed resistances ranging from 100 MΩ to 150 MΩ (measured in a standard external solution) and inner diameter of ≈ 100 nm. High resolution

images were recorded with sharp pipettes, with resistances of ~400 MΩ (range 300-500 MΩ) and estimated inner diameter of ≈ 30 nm. The pipette inner diameters are estimated from the pipette resistance using a half cone angle of 3º**.**

HPICM Resolution

For a detailed description of HPICM resolution, as well as SICM in general, please refer to supplementary materials of Novak et al.[17]. Images from the HPICM were processed to remove minor artifacts using a salt removal method that replaced peak values over a 3x3 lattice with the median value. In addition images were destriped to remove edge artifacts caused by scanning in rectangular blocks. (ScanIc Image, Ionoscope Ltd, version 1.0.0.0).

Simulated Surfaces

Simulated surfaces were created within a stack of 2D images in which voxels were connected to the six neighbours with a shared face. A surface was created by a network of voxels each joined to four, of six possible, neighbours. Individual pillars, with a radius of 8 pixels and uniform height, were added to a flat surface at randomly selected non overlapping positions. Smaller rectangular pillars, 3x3 pixels on a 5x5 pixel base were added at sites with a 5 pixel spacing in the X and Y axes.

Surfaces Derived From HPICM

Height coded images were converted into a 6-connected cubic lattice with lattice nodes equidistant in X,Y and Z, using a stack of 2D images. The original 2D height coded image was converted into a cubic lattice by activating the nodes corresponding to the peak heights. A surface was formed by extending a column of nodes below each peak node to form a connection with each of the four adjacent nodes. Prior to the creation of the cubic lattice, the height coded 2D image was expanded by replicating every pixel three times in the XY plane. This expansion, combined with the method for generating a surface, creates a void within vertical structures that were originally a single pixel wide, preventing tunneling and confining particles to the surface. Individual planes from the cubic lattice were examined and exclusively 8 connected (diagonally) voxels/nodes were, by the addition of a single pixel, connected orthogonally.

Simulated Particle Tracks

An equal probability was assigned to movement to each of the neighbouring orthogonal lattice points with a 50% probability of moving within each cycle The XYZ coordinates were recorded every four cycles with 8 096 records in a track. Particles crossing the bounds of the image rejoined on the opposite side with the flat surfaces embellished with pillars or binding sites. The starting position for tracks on these relatively simple surfaces was selected at random. On the surface of a cell surface (**Fig. 1b**) the start point was randomly selected within the central third of the subregions marked and tracks that exceeded the limits of the surface of the 3D lattice were terminated, and the short track analysed.

The use of Monte Carlo simulation with a 50% move probability is a small departure from the normal 'always move' method. It was chosen because it produces a more realistic probability function (probability against distance): consider a large number of particles at the same starting point on a 2D surface, the always move method moves every particle in the first cycle to the four adjacent pixels and on the second cycle many move back and refill the start point, while others move further out, however the pixels filled after the first cycle are now empty. The start point is occupied and then empty on alternate cycles, which produces an odd probability function. Similarly two particles starting at the same location but on successive cycles can never occupy the same pixel. The 50% move simulation avoids this frenetic

movement and produces a probability functions that more accurately reflect simple diffusion. The downside is that the distances moved are smaller and the computation time is increased, as on average two cycles are required to match the movement of the always move method. However movement over a surface made from connected nodes/voxels in a 3D lattice (stack of 2D images), in which each voxel is connected to four of the six possible orthogonal neighbours, requires that for each move a check is made to establish whether the movement keeps within the surface, it may require up to three tests before a legal move is found.

Note that the movement over the cell surface and over surfaces with pillars is expressed relative to movement on a flat surface, with the same diffusion simulation used in each case.

We do not expect that our method of simulating simple diffusion will have any appreciable affects on the any changes due to topography.

Image Analysis and Simulations

The simulations, generation of the cubic lattice and data analysis were undertaken using software based on a Semper6w (Synoptics, Cambridge, UK) kernel. The scale bar in **Fig. 1e** uses a format[18] which encodes the distance represented within the structure of the scale bar. The number 100 is specified by the presence of short vertical bars at each end of the bar: one vertical bar would indicate 10 and their absence would indicate 1. The units, nm, are specified by the number of small bars on the underside of the bar: 1 for m, 2 for mm and 3 for nm. 3D rendered images were created either with Semper6p (Synoptics), ImageJ (NIH) or ScanIc Image (Ionoscope Ltd). Graphs were created using Excel (Microsoft) and image assembled using Photoshop.

References

1. Yoshigaki, T. *Phys. Rev. E Stat. Nonlin. Soft Matter Phys.* **75**, 041901 (2007).
2. Aizenbud, B.M. & Gershon, N.D. *Biophys. J.* **38**, 287-293 (1982).
3. Aizenbud, B.M. & Gershon, N.D. *Biophys. J.* **48**, 543-546 (1985).
4. Wieser, S. & Schutz, G.J. *Methods* **46**, 131-140 (2008).
5. Hall, D. *Anal. Biochem.* **377**, 24-32 (2008).
6. King, M.R. *J. Theor. Biol.* **227**, 323-326 (2004).
7. Martin, D.S., Forstner, M.B. & Kas, J.A. *Biophys. J.* **83**, 2109-2117 (2002).
8. Ram, S., Prabhat, P., Chao, J., Ward, E.S., Ober, R.J. *Biophys. J.* **95**, 6026-6043 (2008).
9. Parton, R.G. & Hancock, J.F. *Trends Cell Biol.* **14**, 141-147 (2004).
10. Zhang, Y. & Hamill, O.P. *J. Physiol.* **523 Pt 1**, 101-115 (2000).
11. Frick, M., Schmidt, K. & Nichols, B.J. *Curr. Biol.* **17**, 462-467 (2007).
12. Wolf, D.E., Handyside, A.H. & Edidin, M. *Biophys. J.* **38**, 295-297 (1982).
13. Eggeling, C. et al. *Nature* (2008).
14. Day, C.A. & Kenworthy, A.K. *Biochim. Biophys. Acta* **1788**, 245-253 (2009).
15. Karlsson, R., Lassing, I., Höglund, A.S., Lindberg, U. *J. Cell Physiol.* **121**, 96-113 (1984).
16. Sariban-Sohraby, S., Burg, M.B. & Turner, R.J. *J. Biol. Chem.* **259**, 11221-11225 (1984).
17. Novak, P. et al. *Nat. Methods* **6**, 279-281 (2009).
18. Adler, J. *J. Microsc.* **230**, 163-166 (2008).